Femtosecond real-time probing of reactions. IX. Hydrogen-atom transfer

J. L. Herek, S. Pedersen, L. Bañares, and A. H. Zewail
Arthur Amos Noyes Laboratory of Chemical Physics, California Institute of Technology, Pasadena, California 91125

(Received 15 July 1992; accepted 9 September 1992)

The real-time dynamics of hydrogen-atom-transfer processes under *collisionless* conditions are studied using femtosecond depletion techniques. The experiments focus on the methyl salicylate system, which exhibits ultrafast hydrogen motion between two oxygen atoms due to molecular tautomerization, loosely referred to as intramolecular "proton" transfer. To test for tunneling and mass effects on the excited potential surface, we also studied deuterium and methyl-group substitutions. We observe that the motion of the hydrogen, under collisionless conditions, takes place within 60 fs. At longer times, on the picosecond time scale, the hydrogen-transferred form decays with a threshold of 15.5 kJ/mol; this decay behavior was observed up to a total vibrational energy of $\sim 7200\ \mathrm{cm}^{-1}$. The observed dynamics provide the global nature of the motion, which takes into account bonding before and after the motion, and the evolution of the wave packet from the initial nonequilibrium state to the transferred form along the O–H—O reaction coordinate. The vibrational periods ($2\pi/\omega$) of the relevant modes range from 13 fs (the OH stretch) to 190 fs (the low-frequency distortion) and the motion involves (in part) these coordinates. The intramolecular vibrational-energy redistribution dynamics at longer times are important to the hydrogen-bond dissociation and to the nonradiative decay of the hydrogen-transferred form.

I. INTRODUCTION

In this series of papers, the focus has been on real-time femtosecond studies of the nuclear motions in elementary chemical reactions.[1] Usually, bond-breaking and bond-forming dynamics involve the redistribution of electrons between "old" and "new" bonds or the transfer of an electron (harpooning reaction) when the nuclei are in an appropriate configuration. In a whole class of reactions, loosely called proton-transfer reactions, the key to the breaking or making of bonds is hydrogen atom (H) motion or proton (H^+) transfer dynamics, which also occur on the picosecond to femtosecond time scale.

The generic description of these "proton transfer" reactions normally involves a reaction coordinate of the type

$$O_a\text{–H—}O_b, \tag{1}$$

where the light hydrogen nucleus is between two heavy oxygen atoms. With H moving (or transferring) between O_a and O_b, the O_a–H bond is broken and a new one (H–O_b) is formed. This elementary description, which may involve neutral H motion or zwitterion (H^+O^-) formation, is abundant in organic photochemistry and proton-transfer spectroscopy.[2]

Even under collisionless conditions, the motion may not be that simple. The motion of hydrogen on the picosecond or femtosecond time scale may be localized [as in Eq. (1)], or may involve nuclear motions with a simultaneous redistribution of electrons in many bonds. The nature of bonding and electronic charge distribution, as dictated by symmetry rules,[3] frontier orbitals,[4] or the nodal pattern of the wave function,[5] determines the reaction pathway, while intramolecular vibrational-energy redistribution (IVR) plays a role if the nuclei have enough time to change their positions in the course of the reaction.

The femtosecond time resolution is ideally suited for probing the dynamics in such reactions and for initiating the reaction from a localized (nuclear) wave packet. In the gas phase and under collisionless conditions, studies of the initial, intermediate, and final states associated with the H motion could reveal the dynamics in real time. The packet may directly find its way, or may search through other modes for the reaction coordinate, analogous with direct and complex mode reactions.[6]

A prototype large molecular system exhibiting hydrogen transfer is methyl salicylate (MS) where the structure is either ketonic (before the transfer) or enolic (after the transfer). Based on the dual emission spectrum of MS in solutions, which was first investigated in 1924,[7] the idea of proton transfer to form a zwitterionic species (*vide infra*) was proposed by Weller almost forty years ago.[8] Subsequently, a voluminous literature has discussed MS and similar systems (see e.g., Refs. 9–26).

A double-well potential (see Fig. 1) along a reaction coordinate corresponding to the two forms and responsible for the dual fluorescence is an attractive description, because it simplifies the problem considerably. However, in MS, the validity of the double-well model has received considerable attention (see, e.g., Refs. 5, 15, and 23). For example, if a double-well potential description is correct, the tunneling time in the isolated molecule is expected to be $\sim 10^{-7}$ s.[15] Goodman and Brus[15] have shown that in neon matrices at 4.2 K the spectroscopy is not consistent with such a double-well behavior. Picosecond time-resolved studies of isolated MS in a molecular beam by Felker *et al.*,[20] and in solution by Smith and Kaufmann[14] have failed to resolve the dynamics of the transfer, indicating that such a H motion occurs on a time scale less than 10 ps. The time scale of the dynamics and the mechanism

 0021-9606/92/249046-16$06.00

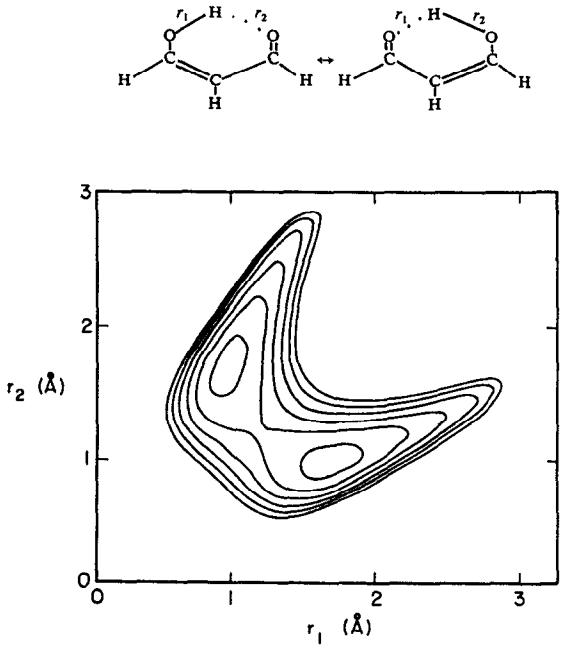

FIG. 1. Two-dimensional potential-energy surface representing a double minimum for malonaldehyde (from Ref. 44). The importance of the two coordinates r_1,r_2 for bond breaking and bond forming processes is analogous to the description of $A+BC$ reactions (see text).

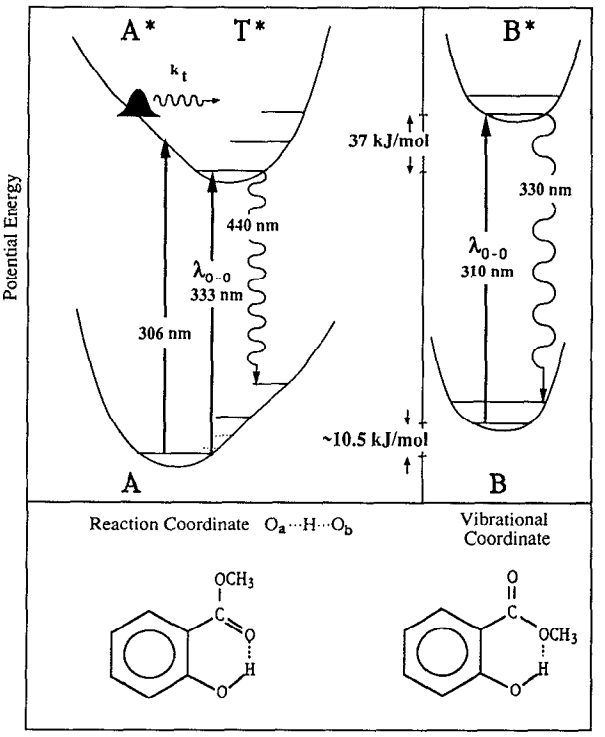

FIG. 2. Schematic representation of the MS system for the "blue" and "uv" rotamers (A and B). In A, the relevant vibrational coordinate of OH stretch (solid line) and C=O and low-frequency mode (dotted lines) are displayed. The wave packet is approximately at the total available energy.

of the reaction depends on the pathway of the motion and, as discussed (*vide infra*) recently by Catalán and coworkers[23] and by Nagaoka and Nagashima,[5] the shape of the potential along the reaction coordinate could be highly asymmetric.

The present work focuses on the femtosecond to picosecond dynamics in isolated MS, building on the earlier studies in the picosecond time domain.[20] The goal is to resolve the elementary reaction dynamics and to examine the associated mechanism of the hydrogen atom transfer. In addition, the coherent nature of the wave packet in a double well or asymmetric potential is of interest as it should reveal the nature of the reaction coordinate and the possible role of IVR. In solutions[27] and clusters,[28] which are not the focus here, there are other interesting questions regarding the role of the solvent and possible intermolecular hydrogen bonding and proton transfer; for examples the reader is referred to the articles in Refs. 27 and 28.

The ground state (A) of MS has a ketonic structure and in the first $^1\pi\pi^*$ state (A^*),[15] the molecule undergoes a transition to a tautomer (T^*) involving a change of the type

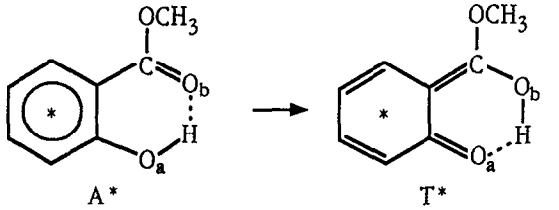

(2)

The excited state (A^*) is similar in structure to A and the ultrafast change from A^* to T^* is responsible for the large Stokes shift observed in the emission spectrum. Originally, Weller attributed the dual fluorescence at 330 nm (so-called uv form) and at 440 nm (blue form) to an equilibrium between the initially excited species and a zwitterion where the carbonyl oxygen receives the proton, giving a positive charge to the carbonyl and leaving behind a negative charge on the phenolic group.[8] This model, which is used in other contexts, turned out to be inapplicable to MS as the uv and blue emissions were found to have distinct excitation spectra in the solution phase,[11,13] in room-temperature vapor,[18] and in supersonic jets.[19] Thus, there is no equilibrium in the excited state, rather, the origin of the dual fluorescence is due to the presence of two rotamers in equilibrium in the ground state, A and B. In rotamer A, the phenolic H is intramolecularly bonded to the carbonyl oxygen, and in rotamer B, to the oxygen of the methoxy group (see Fig. 2). With this in mind, the blue emission is due to an excited state proton-transferred species T^*, originated from rotamer A^*. The uv emission is due to the excited-state B^* species.

A schematic for the potential along the reaction coordinate for A and along the vibrational coordinate for B is displayed in Fig. 2. The experiments in supersonic jets by Helmbrook *et al.*[19] have revealed the high-resolution spectra of both forms and provided important spectroscopic information on the vibrational modes and isotope effect. Nishiya *et al.*[24] have also studied MS and other related compounds and obtained spectroscopic information on the

modes and the potentials. The shape of the potential associated with the O–H—O mode could not be obtained experimentally, as nonradiative decay of the blue form becomes significant at energies below OH stretch frequencies. Semiempirical and "*ab initio*" molecular-orbital (MO) calculations indicate either a small barrier to hydrogen transfer,[22,23] or no barrier at all.[5] The picosecond studies[20] of beam-cooled MS explored the fluorescence decay rate as a function of excess vibrational energy and within this time resolution, an entrance channel barrier to formation of the blue species could not be observed. However, a marked increase in decay rate beyond a threshold of $\sim 1300\ cm^{-1}$ of excess vibrational energy suggested an exit barrier for the onset of an efficient decay channel. This is consistent with the intensity fall off in the excitation spectrum at the same energy found in the gas phase[17a,18] and in supersonic jets.[19] As discussed later, the experiments reported here on isolated MS address the global nature of the surface and the dynamic motion from the early femtosecond times to the picosecond time regime where the onset of this nonradiative process is observed.

The outline of the paper is as follows. In Sec. II, a brief description of the experiment and data analysis method is provided; results are presented in Sec. III. The results are followed by a discussion in Sec. IV. Section IV explores the dynamics of the motion as well as the reaction mechanism. Concluding remarks are given in Sec. V.

II. EXPERIMENTAL

The femtosecond laser system and data processing methods have been described in detail previously.[29] Briefly, the output of a colliding-pulse mode-locked laser (CPM) was amplified in four dye stages pumped by a 20 Hz Nd:YAG laser to yield ~80 fs pulses of energies up to 0.5 mJ and a central wavelength of 610 nm. The pulses were split into two beams of comparable intensity to provide the pump and probe arms. For wavelengths other than the frequency-doubled fundamental of the CPM, the pump beam was tightly focused into a cell of D_2O to produce a white-light continuum, from which twice the desired pump wavelength was selected via a 10 nm bandpass interference filter. The transmitted light was further amplified in a flowing dye cell which was end pumped by residual Nd:YAG 532 nm radiation. The beam was then frequency doubled in a KD*P crystal to produce ultraviolet pump pulses. The pulses generated in this manner had wavelengths in the range of 280–330 nm.

The probe beam was used without modification, as only a single probe wavelength of 610 nm was employed in these experiments. The probe beam was propagated through a Michelson interferometer in which its delay relative to the pump beam was controlled by an actuator. The two beams were then colinearly recombined and focused into the reaction cell. Fluorescence from laser-induced depletion (LID) was collected perpendicular to the propagating beams and dispersed by a 0.33 m monochromator before being detected by a photomultiplier tube. The pump and probe beams were characterized both spectrally and temporally, and the signal linearity was checked throughout the course of this study.

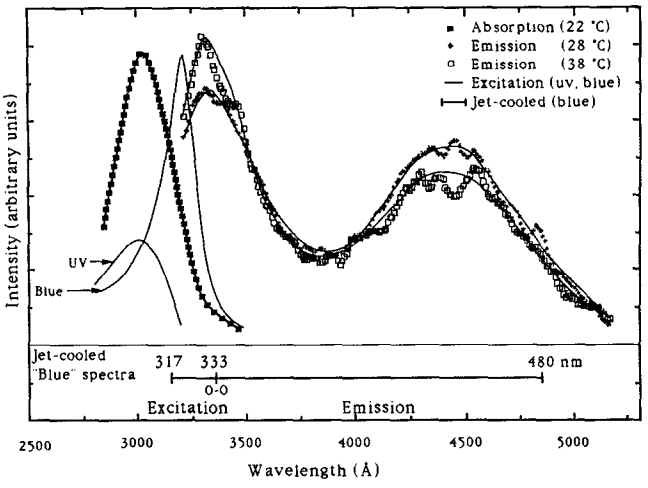

FIG. 3. Absorption, excitation, and experimentally observed emission spectra of room-temperature MS vapor (P=0.2 Torr). The ratio of uv/blue emission increases with increasing thermal energy. ♦, $T\sim 28$ °C; □, $T\sim 38$ °C. Low-resolution (1 nm) absorption and excitation spectra adapted from Ref. 17(a). At the bottom, the spectral range of the emission and excitation spectra in jet-cooled MS is shown.

The MS (Aldrich, 99+%) and methyl 2-methoxybenzoate (Aldrich, 99+%) were used as purchased without further purification. A droplet was placed in a static quartz cell, then degassed and the cell evacuated to 10^{-6} Torr; the vapor pressure of MS is approximately 0.2 Torr at room temperature. For experiments involving monodeuterated MS, a stirred solution of MS in a molar excess of D_2O yielded ~60–90 % of the desired molecule, as confirmed by NMR.

As MS is known to interact strongly with silica,[18] the cell was heated gently to prevent adsorption, especially at the cell windows. Owing to the presence of two MS rotamers in the cell, the relative intensities of the two emission maxima are dependent on the excitation energy, including thermal energy in the ground state, as demonstrated by Klöpffer and Naundorf.[11] This temperature dependence is especially significant in real-time studies, as the measured rates depend on the total energy. Figure 3 shows MS fluorescence spectra obtained at 28 and 38 °C, corresponding to a total thermal vibrational energy of 1140 and 1240 cm^{-1}, respectively.[30] The relative ratio of the uv to blue emission observed in the present work is similar in behavior to that of Ref. 17(a). (Note that this ratio depends on the excitation wavelength and the experimental conditions; the jet result[19] is different from the cell result.) In Fig. 3, the excitation and absorption spectra are shown for comparison.

A. Femtosecond depletion spectroscopy

Unlike the typical pump–probe experiment in which the pump excites the molecule to an intermediate state and the probe then carries it to a final, fluorescing state, here the emitting state is the intermediate. Thus, following excitation of MS by the pump pulse, the subsequent fluores-

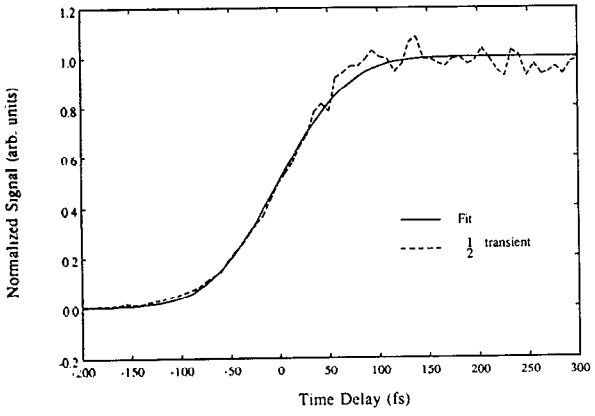

FIG. 4. I_2, 610/(340)/305, transient (dotted line) in the femtosecond time scale. The solid line is obtained by convoluting a single-exponential (I_2, long-time) decay molecular response function with a Gaussian cross-correlation function of 135 fs (FWHM). The measured FWHM of the Gaussian autocorrelation functions for the pump and probe laser pulses are 100 and 90 fs, respectively.

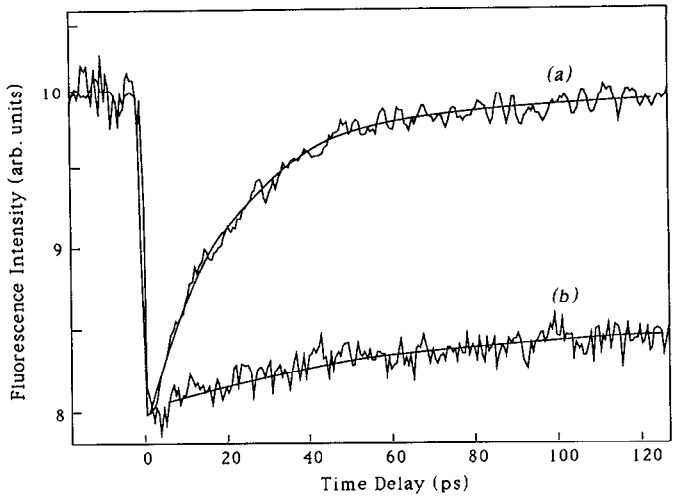

FIG. 5. Experimental depletion results. In both transients, $\lambda_{pu}=305$ nm; $\lambda_{pr}=610$ nm. (a) Detection of 440 nm emission (A form). (b) Detection of 330 nm emission (B form).

cence is *depleted* by the probe pulse. Either the blue or the uv form of MS may be probed, depending on factors such as the pump–probe delay and the excited state dynamics. By measuring the dependence of fluorescence intensity on the relative delay between the pump and probe pulses, we directly monitor the dynamics of the molecule in the excited state. This femtosecond depletion methodology is a variant of the picosecond time domain approach[31] of McDonald and co-workers and Felker and co-workers; here we deplete with a different probe wavelength by absorption to a higher excited state, not back to the ground state. Moreover, the depletion can be made on the initial or final state of the system. With stimulated pumping to the ground state, Chen's group[32] has observed the femtosecond transition-state spectroscopy (FTS) of ozone.

B. Analysis and data treatment

There are two important time regimes relevant to the dynamics considered here: the short-time femtosecond dynamics and the relatively long-time behavior in the picosecond domain. The analysis of the data in the short-time scale is done considering a molecular response function, $M(t_D)$, the transient shape which would be obtained when the pump and probe pulses are infinitely narrow, which is then convoluted with the instrumental response function of the system (see the Appendix for more details). In these experiments, the I_2 transient[33] was used as an internal calibration of the instrumental response function, as its shape is given by the convolution of the pump and probe profiles (instantaneous rise) with a long single-exponential decay function reflecting the very long (microsecond) lifetime of I_2. In addition, the autocorrelation functions of both laser pulses were carefully measured (in the case of the uv pump laser, the residual visible light after the doubling crystal was used) and fit to Gaussian functions.

Figure 4 shows a typical I_2 transient in the short-time scale. The solid line in Fig. 4 is the convolution of a long-time single-exponential decay molecular response function with the Gaussian cross-correlation function whose full width at half maximum (FWHM) is obtained from the measured autocorrelation functions as $F^2_{\text{xcorr}} = F^2_{\text{pump}} + F^2_{\text{probe}}$, where F_i is the FWHM of each function.[34] Using this characterization of the instrumental cross-correlation function, the MS experimental data were fit by convoluting an appropriate molecular response function [see the Appendix, Eq. (A10)] with this cross-correlation function. From simulations, we found that with a Gaussian cross-correlation function of $\sim$130 fs (FWHM), risetimes in the transients as short as $\sim$40 fs can be resolved.

III. RESULTS

The femtosecond dynamics in the excited state of MS were obtained by monitoring fluorescence as a function of time using the depletion method described earlier. Both short and long (up to 120 ps) transient signals were obtained, detecting fluorescence at both emission maxima: 330 and 440 nm. Typical data in the long-time scale are presented in Fig. 5, where the *depletion* of fluorescence resulting from absorption of the probe pulse is clearly demonstrated. The zero of time, in which the pump and probe pulses are temporally overlapped, has been (arbitrarily) set at the onset of depletion. In the case of the 330 nm emission, the lifetime of the corresponding state ($\sim$1.1 ns) [Ref. 17(b)] is very long on our time scale, leaving the excited-state population relatively constant following excitation by the pump pulse. Hence, the depletion by the probe varies little with time delay (on a picosecond time scale). In contrast, the 440 nm emission displays a measurable decay on the picosecond time scale. The decay is represented by a single exponential.

In Fig. 5, the fluorescence signal is decreased when the pump precedes the probe, as expected for a depletion experiment. However, in all following transients, the data are inverted to allow for discussion of the rise and decay components of the depletion in a more conventional manner. Throughout, we shall use (similar to our other FTS pa-

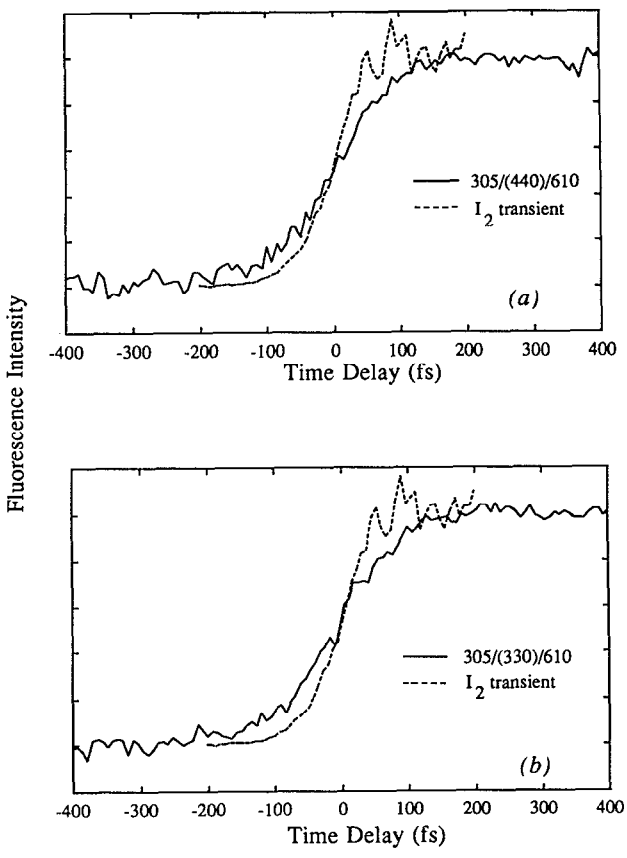

FIG. 6. Fluorescence depletion transients (305/610) detecting the emission at (a) 440 nm and (b) 330 nm, on the femtosecond time scale (solid lines). The I_2 610/(340)/305 transient is also shown for comparison (dotted line). Temperature: 28 °C.

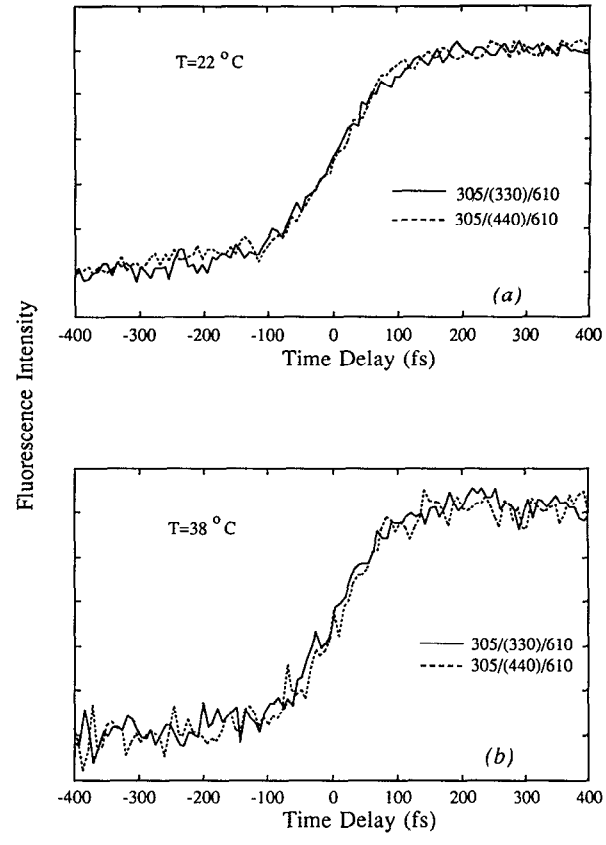

FIG. 7. Effect of the temperature on the transients. The 305/(440)/610 and (330) fluorescence depletion transients in the femtosecond time scale are shown for two different temperatures: (a) 22 °C and (b) 38 °C.

pers[1]) a shorthand notation to indicate the pump, fluorescence-detection, and probe wavelengths, i.e., $\lambda_{pu}/(\lambda_{det})/\lambda_{pr}$. For instance, 305/(440)/610 means that the MS was initially excited with a 305 nm pump laser, and the subsequent fluorescence of the intermediate state at 440 nm was depleted with the 610 nm probe laser.

A. Femtosecond time scale: short-time behavior

Of particular interest to this work is the detection of any rise component in the 440 nm fluorescence depletion transients: such a rise should correspond to the time required for the motion of the hydrogen. For that reason, the temporal behavior of the fluorescence at 330 and 440 nm has been measured on a femtosecond time scale. For these experiments, the pump and probe wavelengths were 305 and 610 nm, respectively, and the thermal vibrational energy was varied by changing the temperature.

Figure 6 shows typical fluorescence depletion transients detecting at 330 and 440 nm. The I_2 transient, reflecting the cross-correlation function of the system, is also shown for comparison. Both MS transients (330 and 440 nm detection) are quite similar and show a slower rise than I_2.[35] Note that the 330 and 440 nm transients have been normalized to allow for comparison. Figure 7 shows how these transients are not affected by variations in temperature. Although the relative intensities of the two emission signals depend on the thermal energy (as discussed in section II), the rise is unaffected.

B. Energy dependence: Long-time behavior

The fluorescence was studied as a function of excitation energy in 10 nm increments from 330 to 280 nm. Throughout this range, the transient observed with 330 nm detection (i.e., fluorescence originating from the uv species) was unaffected by any pump energy variation. With 440 nm detection of the blue species, however, the decay rate is strongly dependent on the pump energy. Figure 8 presents experimental transients obtained with pump wavelengths of $\lambda_{pu}=330$ nm, $\lambda_{pu}=310$ nm, and $\lambda_{pu}=290$ nm, corresponding to excess vibrational energies of 1460, 3650, and 5670 cm^{-1}, respectively.[30] For low energies, the decay had been studied previously[20] via picosecond fluorescence spectroscopy in supersonic beams and the subnanosecond time constants could be measured quite accurately. Here, given the constraint of 120 ps for these femtosecond experimental scans, only the very rapid decays at higher energies could be fitted with reasonable accuracy.

Figure 9 shows the effect of the initial thermal energy on the observed decay and Table I lists the time and rate constants corresponding to excitation energies used both in

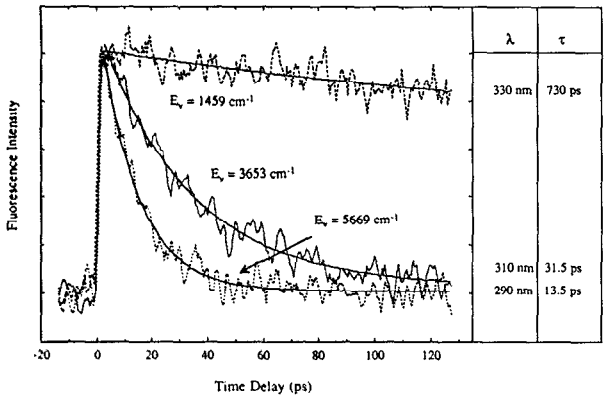

FIG. 8. Transients observed for the 440 nm emission as a function of excitation energy. The solid lines are least-squares single exponential fits to the data, yielding the time constants as shown.

the current work and in previous experiments,[20] where supersonic-cooled MS was studied only up to $E_v = 1850$ cm^{-1}.

C. Deuterium and CH_3 substitution effect

Similar experiments (short- and long-time scales) were performed on two variations of MS: the monodeuterated (MS-D) species, in which the hydrogen of interest is replaced by a deuterium atom, and methyl 2-methoxybenzoate (MS-CH_3), in which the hydrogen is replaced by a methyl group. The MS-D behaved the same as MS. Figure 10 shows transients in both the femtosecond and picosecond time scales, detecting at 440 nm (rotamer

TABLE I. Measured decay time constants and their corresponding rates as a function of excess vibrational energy (E_v).

$E_v(cm^{-1})$(Ref. 30)	τ	k (10^9 s^{-1})	Reference
0	12.0 ns	0.083	Ref. 20[b]
300	10.0	0.100	Ref. 20
911	6.5	0.153	Ref. 20
1043	5.2	0.191	Ref. 20
1225	2.0	0.493	Ref. 20
1312	1.1	0.893	Ref. 20
1459	730 ps[a]	1.4	This work
1573	349	2.86	Ref. 20
1850	160	6.29	Ref. 20
2544	73±20	13.7±2	This work
3653	31.5±4	31±3	This work
4519	21.7±2	46±4	This work
5669	13.5±1.5	73±8	This work
7157	8.5±0.9	119±12	This work

[a]On our picosecond time scale, the transient decay for this experiment was nanosecond in nature. Therefore, the estimated error is large (approximately 50%).
[b]Earlier beam results from this laboratory.

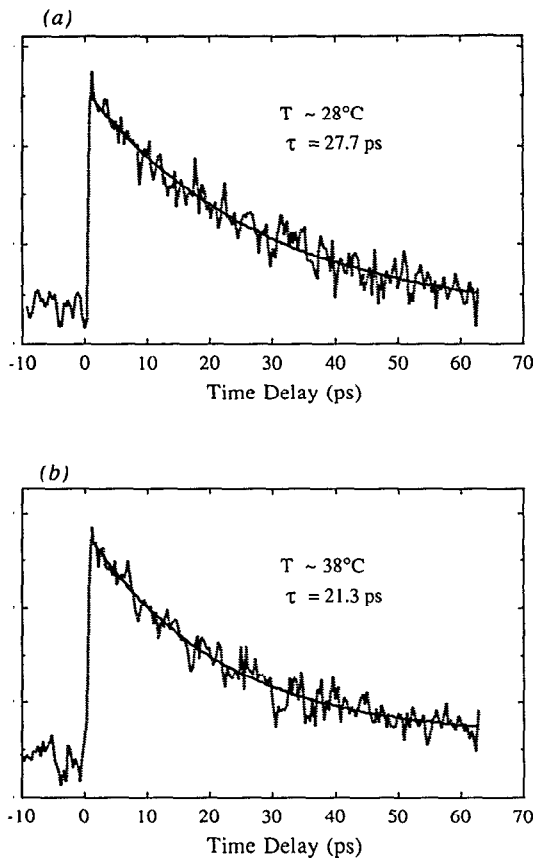

FIG. 9. Effect of temperature on the picosecond transients. Detection of 440 nm emission at (a) $T \sim 28$ °C and (b) $T \sim 38$ °C. The decay rate increases with increasing temperature, as reflected by the time constants τ (see text).

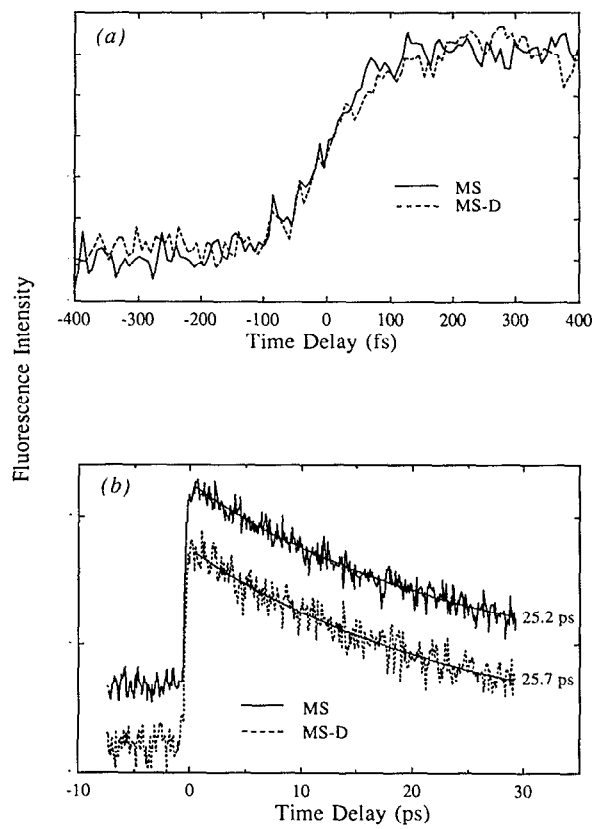

FIG. 10. 305/(440)/610 fluorescence depletion transients for MS and MS-D (isotope effect): (a) short-time scale; (b) long-time scale. Solid line, MS signal; dotted line, MS-D signal.

A). No apparent differences in the rise are observed and the decay rates are identical. As has been previously observed,[8] the MS–CH_3 showed a very different fluorescence spectrum from that of MS: a large peak at 350 nm was followed by a long tail to the red with no second peak at ~440 nm (i.e., no hydrogen dynamics). Depletion of the 350 nm fluorescence emission was analogous to that of the corresponding 330 nm signal of MS, although considerably smaller.

IV. DISCUSSION

The results presented in Sec. III illustrate two dynamical processes in MS, one of which is responsible for the Stokes shifted emission, and the other, for the nonradiative decay in the hydrogen-transferred form. In this section, the origins of these processes are examined with particular focus on the time scale of the elementary step of the reaction and its associated mechanism.

A. Reaction dynamics

1. Preliminaries

Unique excitation spectra of the two rotamers were first recorded by Klöpffer and Naundorf, who also showed that the relative intensity of the two fluorescence bands depends on the excitation wavelength.[11] The structures of the two rotamers *A* and *B* have been studied by Catalán *et al.*,[17] and Pimentel and co-workers.[26] High-resolution emission spectra have been obtained in supersonic beams[20] and in durene crystals (4.2 K).[24] The 0-0 transitions for the uv- and blue-emitting species in the gas phase are at 309.6 and 332.7 nm, respectively. In the ground state, the two species differ in enthalpy by 10.5 kJ/mol;[19] in the excited state, by 37 kJ/mol according to the difference in 0-0 transition energies. Under the assumption that the ratio of the fluorescence reflects the ratio of the population after correcting for the relative transition strengths, it was concluded that the uv form is about 1/70 of the blue in the ground state[19] (note that the blue quantum yield decreases with energy).

The two species exhibit markedly different fluorescence lifetimes. Upon excitation at their respective 0-0 transition energies, $\tau_A = 12.0 \pm 0.5$ ns (Refs. 15 and 20) and $\tau_B = 1.1 \pm 0.2$ ns [Ref. 17(b)]. For rotamer *B*, this value is independent of excitation energy, however, for species *A*, the observed decay time depends on the excitation energy, as will be discussed in Sec. IV B. The state of the blue form has been assigned to a $\pi\pi^*$ transition, based on the oscillator strength, isotope shift, and the mode structure (for discussion, see Refs. 5, 15, and 19). The uv form has been attributed (most likely) as due to $n\pi^*$, again based on spectroscopic and theoretical studies.[5,19] For the blue form, the isotope shift of the transition is -99 cm^{-1} and the prominent vibrational modes relevant here are $\nu_{OH}^{ground} = 3258$ cm^{-1}, $\nu_{OH}^{excited} = 2582$ cm^{-1}, $\nu_{C=O}^{ground} = 1690$ cm^{-1}, $\nu_{C=O}^{excited} = 1094$ cm^{-1}, and low-frequency modes, e.g., 180 cm^{-1} in the ground state and 176 cm^{-1} in the excited state.[19,20]

The relevant potential-energy curves along the O–H—O "reaction coordinate" have been discussed qualitatively and semiquantitatively by various groups.[5,15,18,19,22,23] On the basis of the correlation between the change in OH stretch frequency and the change in bond length, Helmbrook *et al.*, estimated the distance of hydrogen transfer to be 0.1–0.2 Å.[19] The excited state O–H stretch frequency mentioned earlier (and not observed due to nonradiative decay) was estimated to be 2582 cm^{-1} based on the deuterium-induced shift of the 0-0 transition (99 cm^{-1}).

Semiempirical molecular-orbital methods were used by Orttung *et al.*,[22] and by Catalán *et al.*[12,23] in investigations of various ground- and excited-state properties of MS and related molecules. It was found that the shape of the excited-state potential-energy curves strongly depends on the relative distance between the phenolic and carbonyl oxygen atoms (O_p and O_c, respectively).[12,23] Recently, Nagaoka and Nagashima reported "*ab initio*" MO calculations in an analog of MS: *o*-hydroxybenzaldehyde (OHBA).[5a] Their results suggest that a tautomerization from the closed conformer A^* to the tautomer T^* is more likely than an actual proton-transfer process. These results will be discussed in Sec. IV A 3.

Further observations relevant to our study of the hydrogen-transfer dynamics in isolated MS are found in previous time-resolved work. In the picosecond time domain, no rise component of the fluorescence signal in a supersonic beam was measured, setting a lower limit on the rate of hydrogen transfer as 10^{11} s^{-1}, the instrumental response function.[20] These beam experiments are also consistent with the limit deduced in the solution phase.[14]

A culmination of the aforementioned observations together with the measurements presented here gives a reaction coordinate of the type shown in Fig. 2 for the femtosecond dynamics. The vertical transitions represent the 0-0 transition energies of the two species and their associated fluorescence maxima. The elusive hydrogen-transfer rate in rotamer *A* is shown as k_t. The relative energies of the two species are displaced according to the measured enthalpy differences. These data will be used in conjunction with the present results to formulate an understanding of the dynamics discussed in the following sections.

2. Femtosecond dynamics

Given the previous upper limit of 10 ps for the time scale of hydrogen transfer, the present femtosecond experiments focused on the early-time behavior of the fluorescence depletion signal. The observations at early times bring two issues into the dynamics: the nature of the initial coherent packet on the potential and the evolution of the packet with time along the O–H—O (and other) coordinates. Before considering these aspects of the motion, it is useful to obtain the rates (the incoherent trajectories) of the level structure representing the MS system.

A simple kinetic model is used to illustrate the different processes involved in the hydrogen-transfer reaction. The general model is discussed in the Appendix to highlight the new features of the depletion experiments. In the depletion of the blue signal, two rate constants are in-

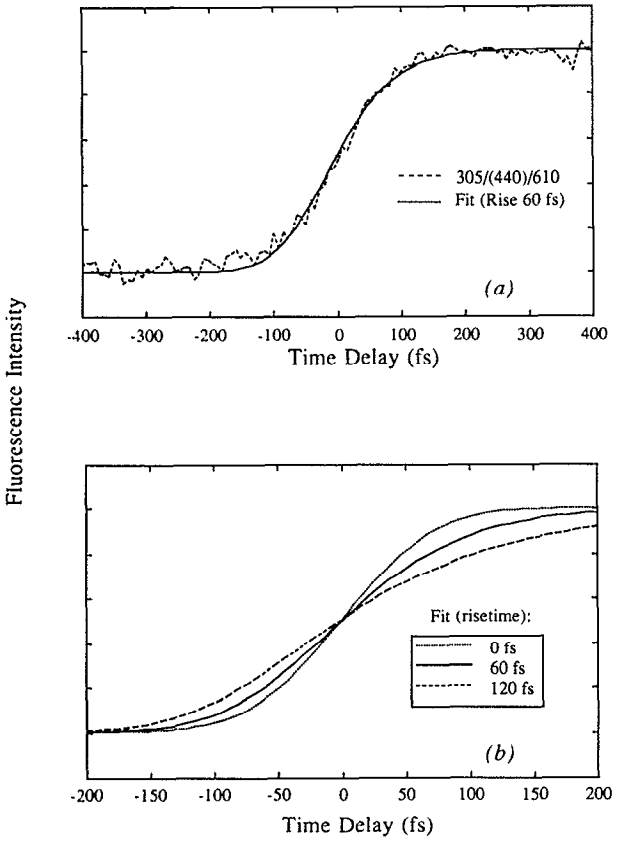

FIG. 11. (a) Typical 305/(440)/610 depletion transient in the femtosecond timescale (dotted line). The solid line is obtained by convoluting a bi-exponential molecular response function (one component in the rise) with the characterized Gaussian cross-correlation function of the system. FWHM (cross-correlation function) = 140 fs; $\tau_{rise} = 60 \pm 10$ fs; $\tau_{decay} = 30$ ps. (b) Several fits are shown corresponding to different risetimes: 0, 60, and 120 fs. The other parameters remain the same.

volved: the hydrogen-transfer rate k_t and the nonradiative rate k_{nr} (see Appendix for schematic illustration, Fig. 15). If the cross section for the hydrogen-transferred state at the probe wavelength λ_{pr} is nonzero but that of the untransferred state A^* is negligible [see Eq. (A10)], and if the hydrogen-transfer rate is much faster than the nonradiative rate, $k_t \gg k_{nr}$, then the depletion of the blue signal at 440 nm will rise with k_t and decay with k_{nr}.

The model also explains why, if $k_t \gg k_{nr}$, the "resonance" fluorescence (which is in the uv, similar to that from B^*) signal from A^* will be several orders of magnitude less than the blue signal. In the experiment, however, the amount of uv fluorescence signal observed is on the same order of magnitude as the blue signal, hence, the total uv signal must be due almost entirely to the emission from B^*. Accordingly, the depletion of the total uv signal should decay with the fluorescence lifetime of B^*. If this fluorescence comes directly from the initially excited state of rotamer B and if fluorescence is the only decay channel, then there will be no additional rise time for the uv depletion other than that due to the finite widths of the laser pulses and the dynamics of the packet from the initial nonequilibrium state prepared by the pump pulse.

Figure 11(a) shows a typical depletion transient for a 305/(440)/610 experiment on the femtosecond time scale. To fit this data, the convolution of a bi-exponential molecular response function (where one of the exponential components is in the rise) with the characterized cross-correlation function of the system was needed (see Sec. II B). The solid line in the plot was obtained including an additional rise time of 60 ± 10 fs. This result, in view of the kinetic model described earlier, would suggest that the 60 fs corresponds to the rate of the hydrogen-transfer process described by k_t.

In the transient of 305/(330)/610, i.e., exactly the same experiment except detecting the fluorescence at 330 nm (non-hydrogen-transferred species B^*), similar rise times and time-zero positions were obtained (to within our resolution). As with rotamer A, when rotamer B is initially pumped from the ground to the excited state by a 305 nm femtosecond photon, a coherent wave packet is produced. This packet requires some time to spread out in the multidimensional potential-energy surface before reaching an appropriate equilibrium region from which the fluorescence is emitted, taking into account the role of Franck–Condon factors. This dispersion of the packet arises as it experiences a large change in the force $(-dV/dR)$ at the vertical excitation. Such dispersions have been observed in elementary systems.[36]

For rotamer A, the evolution of the packet as it moves from the initial nonequilibrium position is similarly explained. The OH stretch period is 13 fs, taking an O–H stretch frequency of 2582 cm^{-1}.[19] Therefore, if the hydrogen movement is less than the vibrational amplitude, then within 60 fs of wave-packet evolution, the "movement" of the hydrogen atom of interest along the reaction coordinate is complete. To better understand the time scale of the motion we have considered three simple representations of the hydrogen-transfer potential.

If the system is moving from the initial nonequilibrium configuration (keto structure) to the hydrogen-transferred configuration (enol structure) as a free particle, then given the available energy of ~ 3900 cm^{-1}, the time for motion is extremely short; a few femtoseconds. If, instead, we take the "repulsive wall" of the asymmetric potential to be exponential, one can calculate the propagation time including the acceleration due to the potential;[1,36,37] in this case, it is ~ 3 fs for a distance span of ~ 0.2 Å.

A more realistic potential is to consider a double well formed from two Morse potentials[38] (or others[39]), but now introduce an asymmetry to the potential. Doing so and integrating the equation of motion resulted in $\tau \sim 4$ fs for a distance of ~ 0.2 Å. In the aforementioned calculations we have assumed that all available energy is in the reaction coordinate. If all modes (for MS, 51) are accepting modes in the packet preparation, then if even one-tenth of the energy ends up in the reaction coordinate, τ will be approximately 10 fs (note for free motion, $\tau \propto E^{-1/2}$).

The aforementioned picture considers the problem as one dimensional, with the H between two oxygens. Considering the O–H—O as a normal mode actually makes the time shorter,[40] but considering the second (and higher) dimensions of the potential is a more realistic step as out-

of-plane low-frequency modes are strongly coupled[41] to the stretch motion. The coupling is due to the large anharmonicity caused by the disparity in masses between hydrogen and oxygen atoms. In a dynamical description, this means that at $t=0$, the packet is coherently prepared in the initial mode(s), but with time it reaches the reaction coordinate by motion in (at least) two dimensions. Such behavior has been observed (as resonance) in elementary[36] and even complex reactions.[42]

For MS in the blue form, the 176 cm^{-1} mode, for example, gives a half period of 90 fs and this is the time scale of interest here. Consistent with experiments, deuterium substitution will not have an effect on this motion (Fig. 10), nor will the excess energy (Fig. 7) as the time scale of the reaction is ultrashort. This description is also supported by the vibronic activity in the hydrogen-transferred form. Felker *et al.*[20] resolved in the emission three types of modes: the low-frequency 180 cm^{-1} progression (built on the 0-0, C=O, and OH stretches, and tentatively assigned as out-of-plane bending motion of the "ring" that includes the intramolecular hydrogen bond); 1690 cm^{-1}, the ground-state carbonyl stretch; and 3220 cm^{-1}, the OH stretch. In the excited state, presumably the 180 cm^{-1} becomes the 176 cm^{-1} and the C=O and O–H undergo reduction to 1094 and 2582 cm^{-1}, respectively, consistent with a hydrogen-transferred form with change in the CO and OH bond order. The excitation spectrum is quite congested at higher energies and certainly at our available energy they must reflect a broadening of at least 60 fs duration.[43] Moreover, the maximum of the emission is displaced by ~ 2 quanta of OH stretch[20] from the 0-0 transition, and the absorption by ~ 1 quantum of OH stretch from the 0-0, giving rise to a net Stokes shift of $\sim 10\,000$ cm^{-1}.[24]

The division of the surface into a two-dimensional (2D) potential, involving two OH bond lengths (the bond being broken and the bond being formed), from the remaining harmonic motions is consistent with the theoretical work by Miller's group on malonaldehyde.[44] In the malonaldehyde case the transfer is coherent in a double well and the estimated splitting is ~ 20 cm^{-1} giving a half period of ~ 1 ps.

The asymmetric potential discussed here for MS is more generic to most systems (than a double-well potential) and one must consider the effect of exoergicity on the redistribution of energy. In the preparation process, IVR will feed energy to the reaction coordinate. In the transfer process, the system is left "hot," and by "exit channel" IVR, the T^* will cool along the reaction coordinate. In other words, the other modes take energy away leaving the reaction coordinate with less energy. The potential in this case must take into account the adiabatic changes of the nuclei and we cannot speak of two coordinates anymore. It would be very interesting to apply Miller's approach to such asymmetric potentials, perhaps dividing the phase space into reactive and nonreactive modes.

The aforementioned result also suggests the absence of any significant barrier in the excited-state potential-energy surface of rotamer *A* as this barrier would result in a coherent trapping and oscillation, or to a delay in the appearance of the H-transferred form, analogous to other systems.[1] As the spreading of the packet in these large systems is also determined by the multidimensionality of the potential, experiments with shorter pulses may lead to faster spreading (and rise) if a coherent state is prepared. As discussed in Sec. IV B, although a barrier is not present for the initial hydrogen transfer, there is a barrier in the exit channel of ~ 15.5 kJ/mol. Rauh[9] has calculated (MO) the keto-enol transformation assuming smooth adjustments as the hydrogen moves and found the minimum to be in the middle of the reaction coordinate. The degree of asymmetry and its position requires more accurate calculations.

3. Proton transfer and tautomerization

Usually, two reaction pathways are used to account for the Stokes shifted emission in systems of this type. The first involves formation of a *zwitterionic* species via a fast, "localized" proton-transfer process, and the second involves distortion of the entire molecular skeleton due to a tautomerization process.

Formation of a *zwitterionic* structure was proposed by Weller[8] and also by Smith and Kaufmann following studies of MS in solution.[14] They suggested that the change in pKa in the excited state of MS induced a complete charge transfer of the phenolic proton to the carbonyl oxygen, accompanied by fluorescence at 440 nm. However, Nagaoka *et al.* showed that the fluorescence decay rate constant is practically independent of the dielectric constant of the solvent.[21] In addition, such a *zwitterionic* structure is likely to be unstable due to Coulombic attraction between the separated charges, unless stabilized by the solvent. The distance between the two oxygen atoms (O_a and O_b) is on the order of 2.5 Å, according to geometry optimization of the excited state.[5a,22,23] The calculated atomic charges on the two oxygen atoms were found to be similar, suggesting that the excited-state molecule is not ionic.[5a]

Recently, a new description of the excited-state dynamics in MS and other intramolecularly hydrogen-bonded molecules has been proposed by Nagaoka and Nagashima.[5] They assert that the nature of the mechanism may be inferred through consideration of the π-system molecular orbitals. The molecule is divided into three groups: the hydroxyl group, the carbonyl group, and the benzene ring. Of these, the benzene ring is the most stable. They then consider the wave functions of the ground and excited states of that individual piece (see Fig. 12). The two excited states of benzene, L_a and L_b, are formed by excitation of an electron from the HOMO to the LUMO, producing the biradicals as shown. The dashed lines represent the nodal planes running perpendicular to the molecular plane.

We now consider the complete MS molecule, the wave function of which largely resembles that of the benzene moiety. In state L_b, the lone electrons localized at *C*1 and *C*4 do not contribute to the *C*2-*C*0 and *C*3-O_p bonds, suggesting a keto configuration which is similar in energy to that of the corresponding benzene wave function. In state L_a, however, the lone electrons at *C*2 and *C*3 stabilize the substituents, facilitating the rearrangement of bonds to

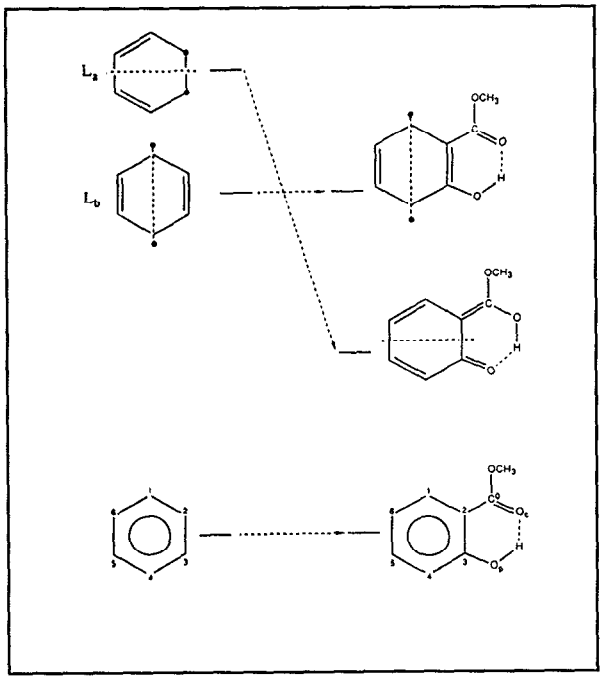

FIG. 12. Nodal plane representation of the MO-based rationalization for excited-state tautomerization, as derived by Nagaoka *et al.* (Ref. 5).

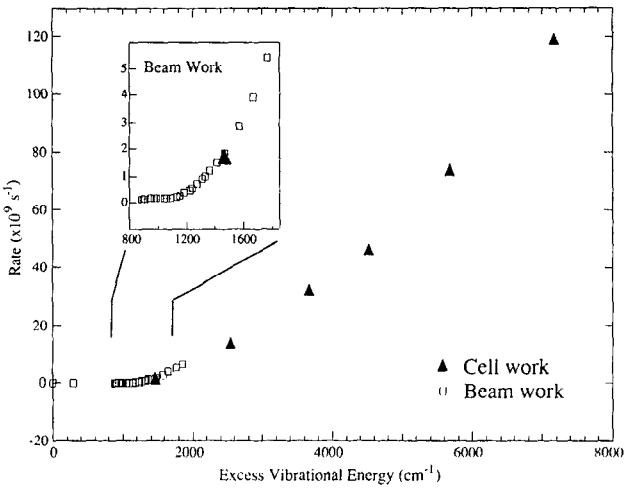

FIG. 13. Decay rate vs excess energy, monitoring the 440 nm emission. The open squares were obtained by Felker *et al.* (Ref. 20), while the solid triangles represent current work. (Inset): Expanded region from 800–1800 cm^{-1}.

produce an enol structure with the hydrogen now shifted toward the carbonyl oxygen (still intramolecularly bonded). This stabilization significantly lowers the energy of the biradical benzyl wave function, thus in the excited state of MS, the tautomer T^* is preferred due to the favorable nodal pattern.

The concept is simple, and is supported by "*ab initio*" MO calculations including geometry optimizations of the ground and first excited states in an analog of MS: *o*-hydroxybenzaldehyde. The optimized geometry of the excited state is consistent with the enol configuration in which the intramolecularly bonded hydrogen is slightly displaced toward the carbonyl oxygen. In these calculations, the hydrogen atom is shown to move toward the carbonyl oxygen by $\sim$0.02 Å upon excitation,[5a] an order of magnitude less than previous estimates.[19] In addition, the O_p–H bond distance increases by only $\sim$0.001 Å, whereas other bond distances and angles are changed significantly. These results are consistent with a molecular tautomerization in which the structural reorganization is not localized, but rather encompasses other degrees of freedom.

A tautomerization would be temporally "instantaneous," as there is an electronic resonance in the aromatic system; thus, there is no large displacement of the hydrogen atom toward the carbonyl oxygen atom upon excitation. This intramolecular bond-electron redistribution is reminiscent of the $A+BC$ chemical dynamics for which simultaneous bond breaking and formation take place. Only if there is an intermediate at a certain nuclear displacement would the system live for longer times than picoseconds. IVR and the nuclear motions "slow down" the dynamics as the system finds (or adjusts during) the reaction coordinate.

B. Nonradiative decay of hydrogen-transferred species

The marked increase of the observed blue decay rate at high excess energies indicates the existence of an efficient intramolecular nonradiative decay process. The picosecond time-resolved studies characterized this behavior in a molecular beam in the range of 0–1850 cm^{-1} of excess vibrational energy;[20] the current work extends this range to $\sim$7160 cm^{-1} beyond the 0-0 transition, as shown in Fig. 13. A threshold energy of $\sim$1300 cm^{-1} marks the onset of the nonradiative channel, in excellent agreement with the activation energy of this channel (15.5 kJ/mol) derived from temperature studies of MS in solution,[14] as well as the decrease in fluorescence quantum yield observed at about this energy.[19]

Dispersed fluorescence spectra of beam-cooled MS revealed a progression of a 180 cm^{-1} mode built on 0, 1690, and 3220 cm^{-1} shifts from the origin,[20] as mentioned earlier. Based on the phenomenological description of a localized hydrogen transfer between the phenolic and carbonyl groups (which are necessarily coplanar with the aromatic ring), Lopez-Delgado and Lazare inferred that the nonradiative decay results from a molecular motion which destroys the coplanarity.[18] An oscillation of the carbonyl group, for example, might couple the excited electronic state to a highly vibrationally excited ground-state level, inducing an internal conversion and/or intersystem crossing.

Based on a similar barrier ($\sim$1200 cm^{-1}) found in the isomerization of stilbene,[45] Felker *et al.*[20] proposed that the onset may be due to the low frequency out-of-plane modes that are often present in "floppy" molecules like stilbene. High-resolution spectroscopic studies by Helmbrook *et al.*,[19] identified this low-frequency mode as belonging to the bridged "ring" containing the intramolecular hydrogen bond; however, they could not associate large-amplitude out-of-plane vibrations with the nonradiative decay (for

discussion, see Ref. 19). In addition, they found that the nonradiative rate depends solely on the excess vibrational energy, not on the excitation of the low-frequency mode.[19]

More recently, Nishiya *et al.*, reported that when the methoxy group on the carbonyl is replaced by other ligands (such as H, CH_3, and NH_2), the low-frequency mode does not appear in the fluorescence spectrum, precluding its association with an out-of-plane bending motion,[24] although matrix effects may be a perturbation here. They suggested that the 180 cm^{-1} mode may be due to internal rotation of the methyl group. Independent of the assignment, if these low-frequency modes are the promoting modes of nonradiative processes, then the decay is a reflection of interelectronic state coupling involving the proximity[46] to nearby states (possible $n\pi^*$ or ground state) or rovibronic couplings as in the channel-3 case of benzene.[47] However, there is another intriguing idea.

In the hydrogen-transferred form of MS, the nascent product is vibrationally hot and the intramolecular hydrogen bond is the weakest. If the effective temperature exceeds a threshold, the intramolecular hydrogen bond will break, leaving the entire moiety (including the methoxy group) "free" to move. Such a process requires a threshold of energy comparable to a typical hydrogen bond strength and because of the "rotation," a large density of states is accessible and helpful to IVR, which enhances the decay. The energy threshold (1300 cm^{-1}) is consistent with previous work[48] in which the minimum energy required for the dissociation of phenol-benzene hydrogen-bonded complex was found to be 1400 cm^{-1}, and is certainly typical of H-bond energies.[39c–39e] For the isoquinoline-water hydrogen bond, the threshold was found to be at $\sim$1000 cm^{-1}.[28a] The accelerated decay can then be understood by considering the increased effective density of states of free or hindered rotation and with methyl group effect on the spectra[49] and on the dynamics of IVR.[50] There is no significant isotope effect (MS-D), consistent with motion above the barrier. IVR-induced decay is known in other systems such as isoquinoline (IQ) and hydrogen bonded IQ–H_2O.[28a,51]

The potential describing both the hydrogen transfer and the breakage (or rotation) of the intramolecular hydrogen bond is depicted in Fig. 14. In a frozen O_a–O_b configuration, the H motion is between the two oxygen atoms, and the potential is similar to that of Fig. 1, with the exception of the asymmetry established from the dynamics. In order to allow for other motions, we must relax this rigidity (away from r_1 and r_2) and let the oxygen (and other) nuclei change position adiabatically. In this case, it is possible to gain a new degree of freedom, e.g., rotation of the OH, or a change in O_a—O_b position, hence leading to new channels. In Fig. 14, we represent the dynamics with a localized exit channel "dissociation" to globally describe the motion of the packet at different vibrational energies. At low energies, the packet moves exoergically toward the well and is trapped. At higher energies, the packet encounters an exit channel barrier, describing the nonradiative decay with the above stretch/rotation H-bond dissociation mechanism.

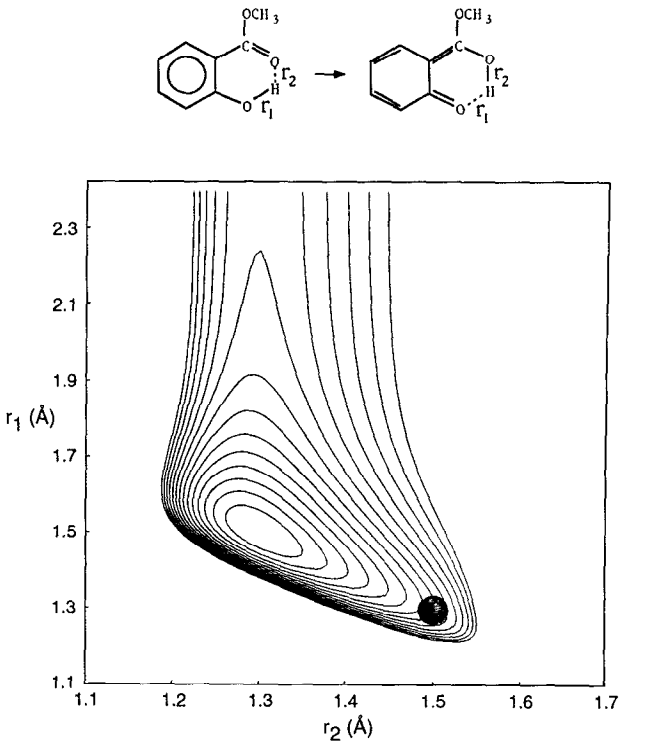

FIG. 14. Schematic two-dimensional potential-energy surface showing both the asymmetry in the potential and the exit barrier to the nonradiative channel. Depending on the total energy, a propagating wave packet (see circle) can either be trapped in the well or exit as the molecule "loses" the hydrogen-bond coordinate (see text).

V. CONCLUSION

The dynamics of hydrogen atom transfer in the gas phase under collisionless conditions are studied using femtosecond depletion spectroscopy. We explore the dynamics from the early femtosecond times to the picosecond time scale, where the hydrogen-transferred species undergoes nonradiative decay. Within 60 fs, the wave packet in MS evolves to cover all configuration space along the reaction coordinate. We observe no deuterium isotope effect, consistent with ultrafast hydrogen movement.

The femtosecond dynamics indicate that intramolecular bond-electron rearrangement involves the molecular framework (nuclear motion and IVR); this process is similar to the case of $A+BC$ reactions where bond breakage and bond formation occur simultaneously. The potential of the motion is highly asymmetric along the O–H—O reaction coordinate. This potential asymmetry, generic to many of these hydrogen-atom transfer reactions, leads to wave-packet motion on a time scale only comparable to the half period of the low-frequency modes, but slower than that of the OH reaction coordinate.

The hydrogen-transferred configuration is observed to undergo a nonradiative decay which depends on the total vibrational energy with a barrier of 1300 cm^{-1}; decay rates were measured up to 7160 cm^{-1}. These observations are related to IVR and to the dissociation (decay) channel linked to the intramolecular-hydrogen bonding. From the

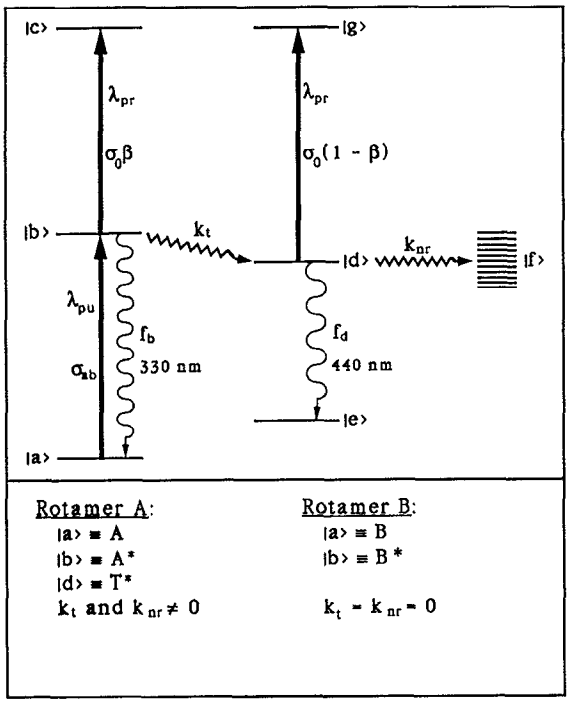

FIG. 15. Schematic of the simple kinetic model. k_t is the transfer rate and k_{nr} is the nonradiative decay rate. The f_i are the fluorescence rates from levels $|i\rangle$. β and σ_0 are defined in the Appendix. The wavelength is denoted by λ and corresponds to the energy difference of the states involved.

dynamics on the femtosecond and picosecond time scales, we deduce the changes in bonding and the associated potential. It would be useful to extend these studies to other interesting systems[52] in a molecular beam.

ACKNOWLEDGMENTS

This work was supported by a grant from the Air Force Office of Scientific Research and by the National Science Foundation. We wish to thank Dr. R. M. Bowman for his initial help with the depletion experiments. We also thank Professors M. Okumura and W. Miller for helpful discussions.

APPENDIX: THE PUMP–PROBE DEPLETION DYNAMICS

A simple kinetic model is presented to illustrate the dynamics of the pump–probe depletion methodology used to relate the transients to the various rates involved. In the kinetic model, the continuous nature of the process on the potential surface is neglected, and instead the reaction is represented by transitions between a number of discrete states, as shown in Fig. 15. This scheme predicts the dependence of the signal on decay rates, power of the pulses, and absorption cross sections. Naturally, to consider the continuous nature of the motion, including coherence effects, the equations of motion must be solved in all configurations, be it done classically, semiclassically, or quantum mechanically.

The model here is similar to that used by Rosker *et al.* in the treatment of FTS.[29] There, however, the pumping and probing were described by rates and the populations were calculated by directly solving all the rate equations, yielding numerical results. In the model here, the pump and probe pulses are first considered instantaneous, and algebraic expressions are obtained for the populations with decay rates appearing explicitly. The calculated signals, which are functions of the time delay between the pump and probe, t_D, will consequently be molecular response functions. These molecular response functions, when later convoluted with both the pump and probe temporal intensity line shapes, yield the predicted transients, i.e., signal vs t_D. The model developed here does not consider stimulated emission and hence cannot describe saturation effects. In the unsaturated regime, in which the present experiments were performed, the model is in exact agreement with that of Rosker *et al.*

The model is applied to the specific problem of the MS rotamer A (or B). For A, predicted transients are derived for the Stokes-shifted (blue) emission at 440 nm of the hydrogen-transferred species T^*, and any uv emission at 330 nm from the excited untransferred species A^* to the ground state.

We will now make the following definitions: $n_i(t)$ is the instantaneous population of state $|i\rangle$; k_t the rate of transfer from state $|b\rangle$ to state $|d\rangle$; f_b the rate of fluorescence (at 330 nm) from state $|b\rangle$ to state $|a\rangle$; f_d the rate of fluorescence (at 440 nm) from state $|d\rangle$ to state $|e\rangle$; k_{nr} is the nonradiative rate away from state $|d\rangle$ to state $|f\rangle$. Furthermore, β is defined as a dimensionless parameter describing the relative ratio of the two possible probe absorptions such that:

$\beta\sigma_0$ is the cross section for probing from state $|b\rangle$ to state $|c\rangle$

and

$(1-\beta)\sigma_0$ is the cross section for probing from state $|d\rangle$ to state $|g\rangle$,

where $0 \leqslant \beta \leqslant 1$ and σ_0 is a constant cross section.

We now wish to find expressions for the populations after both the pump and probe have arrived. To do this, we split the problem into different time regimes and solve for all the populations in each regime.

(i) $t<0$: before the pump arrives;

$n_a(t)=N=$number of molecules in the interaction region,

$n_b(t)=\cdots=n_g(t)=0$.

(ii) $t=0$: the instant the pump arrives; $n_a \rightarrow N-n_0$,

$$n_b \rightarrow n_0 = N\sigma_{ab}\lambda_{pu}E_{pu}/(hc\pi R^2),$$

$$n_c(0)=\cdots=n_g(0)=0,$$

where σ_{ab} is pump absorption cross-section, and the pump has wavelength λ_{pu}, total energy E_{pu}, and is focused to radius R in the interaction region.

(iii) $0<t<t_D$: the system evolves;

$$dn_a/dt=f_b n_b, \tag{A1}$$

$$dn_b/dt=-(k_t+f_b)n_b, \tag{A2}$$

$$dn_d/dt=k_t n_b-(k_{\rm nr}+f_d)n_d, \tag{A3}$$

$$dn_e/dt=f_d n_d, \tag{A4}$$

$$dn_f/dt=k_{\rm nr} n_d, \tag{A5}$$

$$dn_c/dt=0=dn_g/dt. \tag{A6}$$

(iv) $t=t_D$: the probe arrives and depletes states $|b\rangle$ and $|d\rangle$;

$$n_b \rightarrow n_b(t_{D^-})\cdot(1-\alpha\beta\sigma_0),$$

$$n_c \rightarrow n_b(t_{D^-})\cdot\alpha\beta\sigma_0,$$

$$n_d \rightarrow n_d(t_{D^-})\cdot[1-\alpha(1-\beta)\sigma_0],$$

$$n_g \rightarrow n_d(t_{D^-})\cdot\alpha(1-\beta)\sigma_0,$$

where $\alpha=\lambda_{\rm pr}E_{\rm pr}/(hc\pi R^2)$, and the probe has wavelength $\lambda_{\rm pr}$, total energy $E_{\rm pr}$, and radius R equal to that of the pump. The constant α can be thought of as the product of a probe flux and the short time during which it acts, $\alpha=\Phi_{\rm pr}(\Delta t)_{\rm pr}$.

(v) $t>t_D$: the system again evolves according to Eqs. (A1)–(A6).

We can solve for all the populations. In particular, we can find n_a and n_e.

A relevant simplification will be made by imposing the following limits throughout: $f_b \ll k_t$ and $f_d \ll k_{\rm nr}$. The former is justified as the transfer process in MS is expected to occur on the picosecond time scale or less,[14,20] whereas the fluorescence occurs on the nanosecond time scale [$f_b^{-1}\sim 1.1$ ns, Ref. 17(b)]. The latter limitation is valid since the nonradiative lifetime is in the picosecond range, whereas the fluorescence lifetime is in the nanosecond range [$f_d^{-1}=12$ ns, (Ref. 20) and, for instance, at $\lambda_{\rm pu}=305$ nm, we have $(f_d+k_{\rm nr})^{-1}=30$ ps]. Note that these two limits are appropriate for rotamer A only, and that the formulas that follow are not applicable to rotamer B by simply setting k_t to zero, because $f_b \ll k_t$ has been imposed. For rotamer B, it is straightforward to obtain the molecular response function (see Fig. 15).

The uv signal is the total number of molecules that fluoresced from $|b\rangle$ to $|a\rangle$: $M_a(t_D)=n_a(t\rightarrow\infty)-(N-n_0)$. The blue signal is the total number of molecules that fluoresced from $|d\rangle$ to $|e\rangle$: $M_e(t_D)=n_e(t\rightarrow\infty)$.

Solving for the uv signal we get

$$\begin{aligned} M_a(t_D)&=1, \quad t_D<0 \\ &=1-\alpha\beta\sigma_0\exp(-k_t t_D), \quad t_D\geqslant 0 \end{aligned} \tag{A7}$$

and for the blue signal,

$$\begin{aligned} M_e(t_D)&=1, \quad t_D<0 \\ &=1-\alpha\sigma_0\{\beta\exp(-k_t t_D)+K(1-\beta) \\ &\quad\times[\exp(-k_{\rm nr}t_D)-\exp(-k_t t_D)]\}, \quad t_D\geqslant 0 \end{aligned} \tag{A8}$$

where $K=k_t/(k_t-k_{\rm nr})$, and the normalization factors are $n_0 f_b/k_t$ for $M_a(t_D)$ and $n_0 f_d/k_{\rm nr}$ for $M_e(t_D)$. Therefore, for instance, if $k_t \gg k_{\rm nr}$, the uv signal from rotamer A will be orders of magnitude less than the blue fluorescence signal.

Both transients show that the probe acts to decrease (or deplete) the fluorescence if it arrives after the pump, i.e., if $t_D\geqslant 0$. The uv signal is only affected by the probing of $|b\rangle$, and, hence, it depends only on the one rate k_t. The blue signal, however, will depend on two rates. The contribution to the decrease of the blue signal due to the probing of state $|b\rangle$ can only depend on k_t, since this is the effective rate at which molecules leave state $|b\rangle$ to go to $|d\rangle$. The other contribution to the depletion of the blue fluorescence is due to the probing of state $|d\rangle$ and this contribution depends on both rates since, at any time, the population of $|d\rangle$ rises with a rate k_t and decays with a rate $k_{\rm nr}$.

These two molecular response functions are strongly dependent on β, thus three important cases will be discussed to show how the probing cross section ratio $(\beta:1-\beta)$ affects these functions.

1. $\beta=0$

In this limit, we are only probing state $|d\rangle$, the transferred state, and there is no probing of state $|b\rangle$. The molecular response function for the uv signal reduces to

$$M_a(t_D)=1, \quad \text{for all values of } t_D. \tag{A9}$$

The blue signal becomes,

$$\begin{aligned} M_e(t_D)&=1, \quad t_D<0 \\ &=1-\alpha\sigma_0 k_t(k_t-k_{\rm nr})^{-1}[\exp(-k_{\rm nr}t_D) \\ &\quad-\exp(-k_t t_D)], \quad t_D\geqslant 0 \end{aligned} \tag{A10}$$

The uv signal is constant, since no probing of state $|b\rangle$ means no depletion of the signal. The blue signal, however, shows a biexponential behavior, since the amount of depletion is directly proportional to the population of state $|d\rangle$ just as the probe arrives:

$$\begin{aligned} n_d(t=t_{D^-})&=n_0 k_t(k_t-k_{\rm nr})^{-1}[\exp(-k_{\rm nr}t_D) \\ &\quad-\exp(-k_t t_D)]. \end{aligned}$$

The blue fluorescence signal is shown in Fig. 16 for three values of k_t. Here $\alpha\sigma_0=0.2$ and $k_{\rm nr}^{-1}=30$ ps (since $\lambda_{\rm pu}=305$ nm).

2. $\beta=1$

In this limit we are only probing state $|b\rangle$. Then the uv signal is

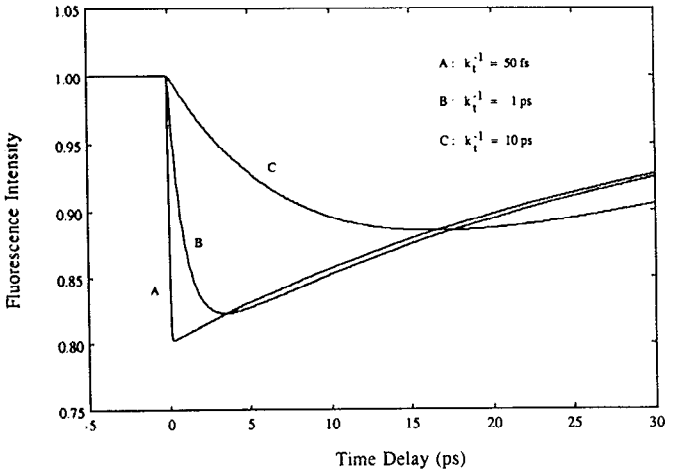

FIG. 16. Molecular response function [Eq. (A10)] for the blue fluorescence from the simple kinetic model for the case $\beta=0$. The response function was calculated using $\alpha\sigma_0=0.2$ and $k_{nr}^{-1}=30$ ps and is shown for three values of the transfer lifetime k_t^{-1}: 50 fs, 1 ps, and 10 ps.

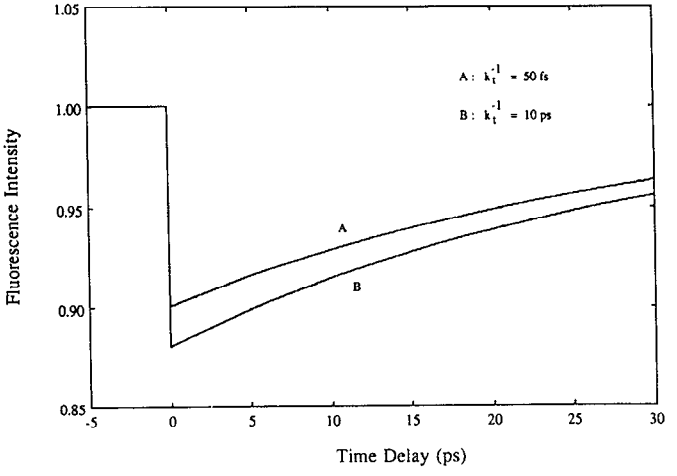

FIG. 18. Molecular response function [Eq. (A14)] for the blue fluorescence from the simple kinetic model for the case $\beta=1/(2-k_{nr}/k_t)$. The response function was calculated using $\alpha\sigma_0=0.2$ and $k_{nr}^{-1}=30$ ps and is shown for two values of the transfer lifetime k_t^{-1}: 50 fs and 10 ps. For this β, the response function is temporally independent of k_t.

$$M_a(t_D)=1, \quad t_D<0$$
$$=1-\alpha\sigma_0\exp(-k_t t_D), \quad t_D\geqslant 0 \tag{A11}$$

and the blue signal is

$$M_e(t_D)=1, \quad t_D<0$$
$$=1-\alpha\sigma_0\exp(-k_t t_D), \quad t_D\geqslant 0. \tag{A12}$$

Thus $M_a(t_D)$ and $M_e(t_D)$ are identical except for the normalization factors given. In this case, the depletion is directly proportional to the population of level $|b\rangle$ just as the probe arrives:

$$n_b(t=t_{D^-})=n_0\exp(-k_t t_D).$$

The blue fluorescence signal is shown in Fig. 17 for various values of k_t and with $\alpha\sigma_0=0.2$. Note the difference in time scale from Fig. 16; k_{nr} and all other parameters were the same.

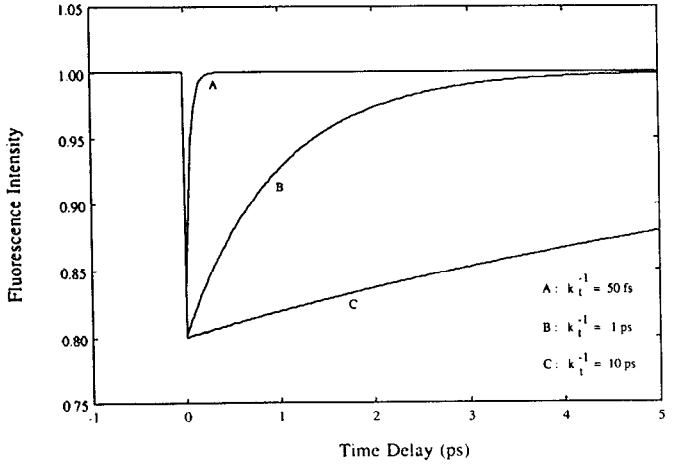

FIG. 17. Molecular response function [Eq. (A12)] for the blue fluorescence from the simple kinetic model for the case $\beta=1$. The response function was calculated using $\alpha\sigma_0=0.2$ and is shown for three values of the transfer lifetime k_t^{-1}: 50 fs, 1 ps, and 10 ps.

3. $\beta=\dfrac{k_t}{k_t-k_{nr}}(1-\beta)$, **i.e.,** $\beta=1/\left(2-\dfrac{k_{nr}}{k_t}\right)$

This can only occur for a value of $\beta\geqslant\frac{1}{2}$. If $k_t\gg k_{nr}$, then this special condition will only be met if $\beta\approx 1/2$.

The uv signal is

$$M_a(t_D)=1, \quad t_D<0$$
$$=1-\alpha\sigma_0\beta\exp(-k_t t_D), \quad t_D\geqslant 0 \tag{A13}$$

and the blue signal is

$$M_e(t_D)=1, \quad t_D<0$$
$$=1-\alpha\sigma_0\beta\exp(-k_{nr} t_D), \quad t_D\geqslant 0. \tag{A14}$$

Notice that in this unique case, the exponential behavior of $M_e(t_D)$ is independent of k_t, the transfer rate. The only dependence on k_t is in β, which of course is fixed for constant k_t. For fixed pump wavelength, k_{nr} and k_t will be fixed, and the aforementioned condition for β specifies what exact value the probing ratio would have to take for the blue signal to be independent of the transfer rate. If β is not close to this value, then the blue signal will have a k_t dependence. Note that the signal that results from this molecular response function (upon convolution with the pulses as described below) has only a decay rate: the rise reflects only the effect of the finite width of the pulses. The blue fluorescence molecular response function is shown in Fig. 18 for $k_{nr}^{-1}=30$ ps and with $\alpha\sigma_0=0.2$.

Finally, the transient signal $A(t_D)$ corresponding to a molecular response function $M(t_D)$ is obtained by convoluting $M(t_D)$ with the temporal intensity shapes of the pump and probe pulses. Therefore, the signal which takes into account the finite width of the pump and probe is

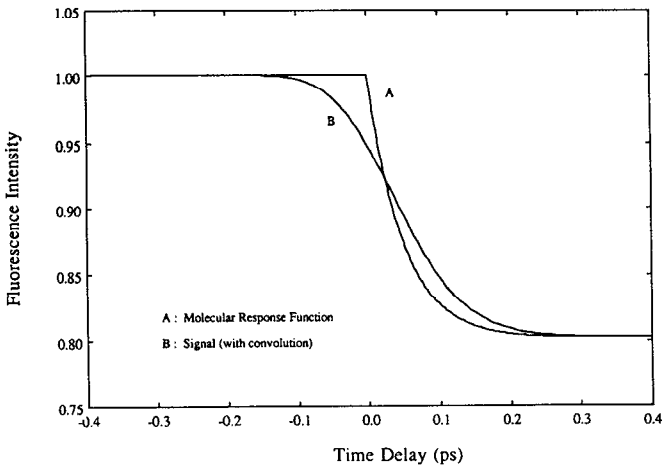

FIG. 19. Blue fluorescence signal from the simple kinetic model for the case $\beta=0$. The molecular response function [Eq. (A10)] has been convoluted with the pump and probe temporal pulse shapes to yield the signal (compare with Fig. 16). Here $\alpha\sigma_0=0.2$, $k_{nr}^{-1}=30$ ps, FWHM = 100 fs for both pump and probe, and the signal is shown for a transfer lifetime k_t^{-1} of 50 fs.

$$A(t_D)=\int_{-\infty}^{\infty} dx\, I_{pr}(t_D-x) \times \int_{-\infty}^{\infty} dy\, M(y) I_{pu}(x-y), \qquad \text{(A15)}$$

where (with $i=1\Rightarrow$pump, $i=2\Rightarrow$probe) the pulse intensities, for example, Gaussian, are

$$I_i(z)=(1/\sigma_i\sqrt{2\pi})\exp\left(-\frac{z^2}{2\sigma_i^2}\right) \qquad \text{(A16)}$$

and the pulse temporal standard deviations are given by

$$\sigma_i=\text{FWHM}_i/2\sqrt{2\ln 2}.$$

The factor $E_i/(\pi R^2)$ in $I_i(z)$, where E_i is the total pulse energy, has been omitted in order to normalize $A(t_D)$.

To show the effect in Eq. (A15), we convoluted $M_e(t_D)$ with the pump and probe intensity shapes to yield $A_e(t_D)$ for the case $\beta=0$, and $\text{FWHM}_i = 100$ fs ($i=1,2$). The signal $A_e(t_D)$ is shown in Fig. 19 for $k_t^{-1}=50$ fs and with $\alpha\sigma_0=0.2$ and $k_{nr}^{-1}=30$ ps.

[1] For recent reviews, see, A. H. Zewail, Faraday Discuss. Chem. Soc. **91**, 207 (1991); L. R. Khundkar, A. H. Zewail, Ann. Rev. Phys. Chem. **41**, 15 (1990), and references therein.
[2] M. Kasha J. Chem. Soc., Faraday Trans. 2 **82**, 2379 (1986).
[3] R. Hoffmann and R. B. Woodward, J. Am. Chem. Soc. **87**, 2046 (1965); *The Conservation of Orbital Symmetry* (Academic, New York, 1970).
[4] H. Fujimoto and K. Fukui, *Advances in Quantum Chemistry*, Vol. 6, edited by P. O. Löwdin (Academic, New York, 1972); K. Fukui, Angew. Chem. Int. Ed. Engl. **21**, 801 (1982); R. G. Pearson, Acc. Chem. Res. **4**, 152 (1971).
[5] (a) S. Nagaoka and U. Nagashima, Chem. Phys. **136**, 153 (1989); (b) S. Nagaoka, U. Nagashima, N. Ohta, and T. Takemura, J. Phys. Chem. **92**, 166 (1988); (c) S. Nagaoka and U. Nagashima, *ibid.* **94**, 1425 (1990); (d) U. Nagashima, S. Nagaoka, and S. Katsumata, *ibid.* **95**, 3532 (1991); (e) S. Nagaoka and U. Nagashima, *ibid.* **95**, 4006 (1991).
[6] D. R. Herschback, Angew. Chem. Int. Ed. Engl. **26**, 1221 (1987).
[7] J. K. M. Marsch, J. Chem. Soc. **125**, 418 (1924).
[8] A. Weller, Z. Elecktrochem. **60**, 1144 (1956); Prog. React. Kinet. **1**, 188 (1961).
[9] R. D. Rauh, Ph.D. thesis, Princeton University, 1972.
[10] P. J. Kovi, C. L. Miller, and S. G. Schulman, Anal. Chim. Acta **61**, 7 (1972).
[11] W. Klöpffer and G. Naundorf, J. Lumin. **8**, 457 (1974); W. Klöpffer and G. Kaufmann, J. Lumin. **20**, 283 (1979).
[12] J. Catalán and J. I. Fernandez-Alonso, J. Mol. Struct. **27**, 59 (1975); J. Catalán and F. Tomas, Adv. Mol. Relaxation Processes **8**, 87 (1976).
[13] K. Sandros, Acta Chem. Scand., Ser. A **30**, 761 (1976).
[14] K. K. Smith and K. J. Kaufmann, J. Phys. Chem. **82**, 2286 (1978).
[15] J. Goodman and L. E. Brus, J. Am. Chem. Soc. **100**, 7472 (1978).
[16] D. Ford, P. J. Thistlewaite, G. J. Woolfe, Chem. Phys. Lett. **69**, 246 (1980).
[17] (a) A. U. Acuña, F. Amat-Guerri, J. Catalán, and F. González-Tablas, J. Phys. Chem. **84**, 629 (1980); (b) A. U. Acuña, J. Catalán, and F. Toribio, *ibid.* **85**, 241 (1981); (c) J. Catalán, F. Toribio, and A. U. Acuña, *ibid.* **86**, 303 (1982); (d) F. Toribio, J. Catalán, F. Amat-Guerri, and A. U. Acuña, *ibid.* **87**, 817 (1983); (e) A. U. Acuña, F. Amat-Guerri, F. Toribio, and J. Catalán, J. Photochem. **30**, 330 (1985).
[18] R. Lopez-Delgado and S. Lazare, J. Phys. Chem. **85**, 763 (1981).
[19] L. Helmbrook, J. E. Kenny, B. E. Kohler, and G. W. Scott, J. Chem. Phys. **75**, 5201 (1981); J. Phys. Chem. **87**, 280 (1983).
[20] P. M. Felker, W. R. Lambert, and A. H. Zewail, J. Chem. Phys. **77**, 1603 (1982).
[21] S. Nagaoka, N. Hirota, M. Sumitani, K. Yoshihara, E. Lipczynska-Kochany, and H. Iwanura, J. Am. Chem. Soc. **106**, 6913 (1984).
[22] W. H. Orttung, G. W. Scott, and D. Vosooghi, J. Mol. Struct. **109**, 161 (1984).
[23] M. Sánchez-Cabezudo, J. L. G. De Paz, J. Catalán, and F. Amat-Guerri, J. Mol. Struct. **131**, 277 (1985).
[24] T. Nishiya, S. Yamauchi, N. Hirota, M. Baba, and I. Hanazaki, J. Phys. Chem. **90**, 5730 (1986).
[25] M. M. Radhi and M. F. El-Bermani, Spectrochimica Acta **46A**, 33 (1990).
[26] E. Orton, M. A. Morgan, and G. C. Pimentel, J. Phys. Chem. **94**, 7936 (1990).
[27] See, e.g., P. F. Barbara and H. P. Trommsdorff, Chem. Phys. **136**(2), (1989); P. F. Barbara, P. K. Walsh, and L. E. Brus, J. Phys. Chem. **93**, 29 (1989); P. F. Barbara, G. C. Walker, and T. P. Smith, Science **256**, 975 (1992); P. F. Barbara, P. M. Rentzepis, and L. E. Brus, J. Am. Chem. Soc. **102**, 2786 (1980); T. Elsaesser, W. Kaiser, and W. Lüttke, J. Phys. Chem. **90**, 2901 (1986).
[28] See, e.g., (a) P. M. Felker and A. H. Zewail, J. Chem. Phys. **78**, 5266 (1983); (b) O. Cheshnovsky and S. Leutwyler, *ibid.* **88**, 4127 (1988); (c) R. Knochenmuss, O. Cheshnovsky, and S. Leutwyler, Chem. Phys. Lett. **144**, 317 (1988); (d) T. Droz, R. Knochenmuss, and S. Leutwyler, J. Chem. Phys. **93**, 4520 (1990); (e) J. J. Breen, L. W. Peng, D. M. Willberg, A. Heikal, P. Cong, and A. H. Zewail, *ibid.* **92**, 805 (1990); (f) T. C. Swinney and D. F. Kelley, J. Phys. Chem. **95**, 2430 (1991); (g) J. A. Syage and J. Steadman, J. Chem. Phys. **95**, 2497 (1991); (h) S. K. Kim, S. Li, and E. R. Bernstein, *ibid.* **95**, 3119 (1991).
[29] M. J. Rosker, M. Dantus, and A. H. Zewail, J. Chem. Phys. **89**, 6113 (1988).
[30] Note that the actual excess energy does not simply correspond to $E_{pu}-E_{00}$ (where $\lambda_{00}=332.7$ nm) (Ref. 19) but rather must include the thermal vibrational energy of the ground state MS. The frequencies of the fifty-one vibrational modes were compiled from various sources (Refs. 25 and 26) and the average vibrational energy as a function of temperature was calculated according to $E_{vib}=\sum_{i=1}^{3n-6} h\nu_i/[\exp(h\nu_i/kT)-1]$. At 38 °C, for example, the average thermal vibrational energy is ~ 1250 cm^{-1}.
[31] M. J. Cote, J. F. Kauffman, P. G. Smith, and J. D. McDonald, J. Chem. Phys. **90**, 2865 (1989); T. C. Corcoran, L. L. Connell, G. V. Hartland, P. W. Joireman, R. A. Hertz, and P. M. Felker, Chem. Phys. Lett. **170**, 139 (1990).
[32] Y. Chen, L. Hunziker, P. Ludowise, and M. Morgen, J. Chem. Phys. **97**, 2149 (1992).
[33] R. M. Bowman, M. Dantus, and A. H. Zewail, Chem. Phys. Lett. **161**, 297 (1989); R. M. Bowman, M. Dantus, and A. H. Zewail, Chem. Phys. Lett. **174**, 546 (1990).
[34] The I_2 transients show oscillatory behavior due to the probing of mo-

lecular vibrations (see Ref. 33 for more details). These oscillations were much less pronounced (pump laser 610 nm) in the present work (at the depletion power used) most likely due to absorption from both turning points. There was no measurable distortion in the transients, especially in the rise, at these powers.

[35] Notice that both MS depletion transients were measured in a sequence using the same cell and same pump and probe lasers; the only change was in the position of the monochromator grating (330 vs 440 nm detection). The transients did not show any relative shift, i.e., both MS transients display time zero at exactly the same position. The time zero of the I_2 610/(340)/305 signal could not be compared with that of MS, as it required using a different cell. Therefore, we shifted the I_2 transient such that both (I_2 and MS) coincide, where time zero has been set at half of the rise.

[36] See, e.g., G. Roberts and A. H. Zewail, J. Phys. Chem. **95**, 7973 (1991); P. Cong, A. Mokhtari and A. H. Zewail, Chem. Phys. Lett. **172**, 109 (1990).

[37] R. Bersohn and A. H. Zewail, Ber. Bunsenges Phys. Chem. **92**, 373 (1988).

[38] V. I. Goldanskii, Ann. Rev. Phys. Chem. **27**, 85 (1976).

[39] See, for example, (a) R. Schroeder and E. R. Lippincott, J. Phys. Chem. **61**, 921 (1957); (b) R. L. Somorjai and D. F. Hornig, J. Chem. Phys. **36**, 1980 (1962); (c) Th. Arthen-Engeland, T. Bultmann, N. P. Ernsting, M. A. Rodriguez, and W. Thiel, Chem. Phys. **163**, 43 (1992); (d) G. C. Pimentel, *The Hydrogen Bond* (Reinhold, New York, 1960); (e) *Hydrogen Bonding*, edited by S. N. Vinogradov and R. H. Linnell (Van Nostrand Reinhold, New York, 1971); (f) *Hydrogen Bonds*, edited by P. Schuster (Springer-Verlag, Berlin, 1984).

[40] Using a normal mode analysis (see p. 72 of *Mechanics, 3rd ed.*, edited by L. D. Landau and E. M. Lifshitz (Pergamon Press, Oxford, 1976), Vol. 1, for O–H—O antisymmetrical vibration, the frequency is $\sim \sqrt{2}$ times greater than that of an O–H vibration alone.

[41] F. Laermer, T. Elsaesser, and W. Kaiser, Chem. Phys. Lett. **148**, 119 (1988).

[42] Work in this laboratory on the isomerization of stilbene; S. Pedersen, L. Bañares, and A. H. Zewail, J. Chem. Phys. **97**, 8801 (1992).

[43] Note that the absorption spectrum extends to more energies than the excitation spectrum due to nonradiative decay reflected in the latter (see Fig. 3).

[44] T. Carrington and W. H. Miller, J. Chem. Phys. **84**, 4364 (1986).

[45] J. A. Syage, P. M. Felker, and A. H. Zewail, J. Chem. Phys. **81**, 4706 (1984); L. Bañares, A. A. Heikal, and A. H. Zewail, *ibid.* **96**, 4127 (1992).

[46] E. C. Lim, in *Excited States*, edited by E. C. Lim, (Academic, New York, 1977), Vol. 3, p. 305.

[47] U. Schubert, E. Riedle, H. J. Neusser, and E. W. Schlag, J. Chem. Phys. **84**, 6182 (1986).

[48] J. L. Knee, L. R. Khundkar, and A. H. Zewail, J. Chem. Phys. **87**, 115 (1987).

[49] For an excellent review, see, M. Ito, J. Phys. Chem. **91**, 517 (1987).

[50] C. S. Parmenter and B. M. Stone, J. Chem. Phys. **84**, 4710 (1986); **86**, 51 (1987); J. S. Baskin, T. S. Rose, and A. H. Zewail, *ibid.* **88**, 1458 (1988).

[51] J. L. Knee, L. R. Khundkar, and A. H. Zewail, J. Phys. Chem. **89**, 3201 (1985); P. M. Felker and A. H. Zewail, Chem. Phys. Lett. **94**, 454 (1983).

[52] M. Lee, Y. T. Yardley, and R. M. Hochstrasser, J. Phys. Chem. **91**, 4621 (1987), and references therein; B. J. Schwartz, L. A. Peteanu and C. B. Harris, *ibid.* **96**, 3591 (1992); A. Ito, Y. Fujiwara, and M. Itoh, J. Chem. Phys. **96**, 7474 (1992), and references therein.